JOURNAL OF AIRCRAFT
Vol. 31, No. 6, November–December 1994

Engineering Transition Prediction for a Hypersonic Axisymmetric Boundary Layer

J. Stilla*
DLR—German Aerospace Research Establishment, 38108 Braunschweig, Germany

The hypersonic flow over a blunt, slender cone at $M_\infty = 8$ and $\alpha = 0$ deg is investigated from an engineering point of view. Therefore, the steady, laminar mean flow is efficiently computed by means of an Euler/boundary-layer method that includes second-order boundary-layer theory. Transition prediction is done using local, linear stability theory together with the e^N method. Mean flow, stability results, and transition location are in good agreement with those of other theoretical studies using Navier-Stokes mean-flow solutions. Results of a sensitivity study show the importance of viscous-inviscid interaction and entropy-layer resolution, whereas the use of different viscosity laws had less effect than expected.

Nomenclature

A = disturbance amplitude
b = streamwise length along body surface, m
DDT = second derivative of T, K/m^2
e = internal energy
f = frequency, kHz
L = body length, m
l = Blasius length, $\sqrt{(vb)/u}$, m
M = Mach number
N = N factor
Pr = Prandtl number
p = static pressure
R = gas constant for air, 287 J/(kg K)
$Re_{x,e}$ = local Reynolds number based on outer-edge condition and b, $(u_e b)/v_e$
$Re_{x,\infty}$ = local Reynolds number based on freestream condition and l, $(u_\infty l_\infty)/v_\infty$
Re_∞ = Reynolds number based on freestream condition and RN, $(u_\infty RN)v_\infty$
RN = nosetip radius, m
s = entropy, J/(kg K)
T = temperature, K
v^i = velocity components in x^i direction
x^i = curvilinear coordinates
α = angle of attack, deg
$-\alpha_i$ = spatial amplification rate, 1/m
δ = boundary-layer thickness
δ_1 = displacement thickness
ε = perturbation parameter
Θ_c = cone half angle, deg
μ = dynamic viscosity, kg/(m s)
ρ = density, kg/m^3
v = kinematic viscosity, m^2/s
Ψ = wave angle, deg

Subscripts
e = boundary-layer outer-edge condition
inv = inviscid solution
ref = reference condition
trans = transition location
wall = wall condition
0 = start of integration path
1 = end of integration path
∞ = freestream condition

Presented as Paper 93-5114 at the AIAA 5th International Aerospace Planes and Hypersonics Technologies Conference, Munich, Germany, Nov. 30–Dec. 3, 1993; received Feb. 5, 1994; revision received April 29, 1994; accepted for publication April 29, 1994.

*Research Engineer, Institute of Design Aerodynamics, Lilienthalplatz 7.

Introduction

FOR the design of future hypersonic aerospace planes the estimation of maximum heat loads plays an important role. It especially depends on boundary-layer transition for which engineering tools are required. At the present time an estimation of transition location in hypersonic flow still has to rely on either empirical correlations based on mean-flow properties, or on local, linear stability analysis in conjunction with the e^N method. In any case, a laminar, steady mean flow has to be computed.

Each modification of the design requires repeated transition prediction and, therefore, repeated computation of laminar, steady mean flows. Because solutions of the full Navier-Stokes equations are very time consuming, and therefore expensive, one has to choose an appropriate approximation of these equations. Two common approximations are the parabolized Navier-Stokes equations (PNS) and the thin-layer Navier-Stokes equations (TLNS). Even solutions of these sets of equations have the disadvantage of large CPU-time requirements. Therefore, having engineering demands in mind, an Euler/boundary-layer model including second-order boundary-layer theory may be a suitable alternative.[1,2] Such an approach is used in the work presented here.

Thus far, local, linear stability theory in conjunction with the e^N method for transition prediction has been extensively used for the wing design of civil transport aircrafts, or for the development of laminar flow control techniques.[3] Therefore, it was decided to utilize this method for investigations in hypersonic flow as well. In contrast to sub- and transonic flow, this approach has not yet been sufficiently validated. The problem is that there are not many hypersonic experiments conducted in "quiet" wind tunnels. In addition, transition mechanisms in hypersonic flow are not known in detail.

As the test configuration, a blunt, slender cone at $M_\infty = 8$ and $\alpha = 0$ deg has been chosen. For this configuration both experimental and theoretical references are available for comparison.[4–7] All theoretical stability results known in the literature are based on Navier-Stokes mean flows and local, linear stability theory.

The objective of the work presented here is to investigate whether stability and transition computations based on an Euler/boundary-layer mean flow lead, at significantly less cost, to results comparable to those based on Navier-Stokes solvers. In this context the sensitivity of mean flow, stability, and

transition computation to parameters like viscous-inviscid interaction, entropy-layer resolution, and the utilized viscosity law is of interest also.

Euler/Boundary-Layer Model

The model used here solves the second-order boundary-layer equations. Solutions of this set of equations can be regarded as classical boundary-layer solutions corrected so that wall curvature, viscous-inviscid interaction, and wall-normal inviscid flow gradients are taken into account. The set of second-order boundary-layer equations can be derived by an order-of-magnitude analysis of the Navier-Stokes equations, or by the "matched asymptotic expansion" approach.[1,2,8]

The latter has the advantage of providing information concerning boundary conditions and defining the sequence of Euler and boundary-layer calculations. The flowfield is divided into an inner viscous and an outer inviscid domain. In both, asymptotic expansions of the Navier-Stokes solution in terms of a small ε, which is proportional to $1\sqrt{Re}$, are made.

Substituting these expansions into the Navier-Stokes equations and retaining terms of order $\mathbb{O}(1)$ lead to the classical boundary-layer equations of Prandtl in the inner domain, and the Euler equations in the outer domain, both with their well-known boundary conditions.

Keeping terms up to $\mathbb{O}(\varepsilon)$ leads to inviscid perturbation equations valid in the outer domain, which can be rewritten as Euler equations. Matching of the inner viscous flow to the outer inviscid flow reveals that this perturbation takes into account the displacement effect of the first-order boundary layer. This is done by changing the wall boundary condition. Instead of the classical Euler wall boundary condition $[(v^3_{\text{inv}})_{\text{wall}} = 0]$, an outflow condition is used $[(\rho_{\text{inv}} v^3_{\text{inv}})_{\text{wall}} \neq 0]$. It is calculated so that the displacement surface becomes a stream surface of the Euler solution. The source is proportional to the first derivative in the x^1 direction of the boundary-layer mass-flow deficit.[8-10] In two-dimensional, first-order boundary-layer flow the source is computed as

$$(\rho_{\text{inv}} v^3_{\text{inv}})_{\text{wall}} = \frac{\partial}{\partial x^1}\left[\int_0^{\delta} (\rho_{\text{inv}} v^1_{\text{inv}} - \rho v^1)\, \mathrm{d}x^3\right] \tag{1}$$

Equation (1) written in terms of δ_1 leads to

$$(\rho_{\text{inv}} v^3_{\text{inv}})_{\text{wall}} = \frac{\partial}{\partial x^1}(\rho_{\text{inv}} v^1_{\text{inv}} \delta_1) \tag{2}$$

In the inner domain terms of $\mathbb{O}(\varepsilon)$ lead to viscous perturbation equations that can be rewritten as the so-called second-order boundary-layer equations. Curvature terms are explicitly included and the momentum equation in the wall-normal direction does not vanish. Matching of the inner viscous flow to the outer inviscid flow results in new boundary-layer edge conditions. The inner viscous flow is patched to the outer inviscid flow at δ:

$$\begin{aligned} v^1(x^1, x^2, \delta) &= v^1_{\text{inv}}(x^1, x^2, \delta) \\ v^2(x^1, x^2, \delta) &= v^2_{\text{inv}}(x^1, x^2, \delta) \\ p(x^1, x^2, \delta) &= p_{\text{inv}}(x^1, x^2, \delta) \\ e(x^1, x^2, \delta) &= e_{\text{inv}}(x^1, x^2, \delta) \end{aligned} \tag{3}$$

These "patching conditions" take into account not only inviscid flow gradients within the boundary layer, but also vorticity gradients and changes of the inviscid flow from first- to second-order.[2]

With the preceding in mind, it follows that for solving second-order boundary-layer equations including the displacement effect, one needs the perturbed Euler solution. This is only available in conjunction with a first-order boundary-layer calculation that provides the source distribution. For that purpose inviscid wall values of an unperturbed Euler solution are needed. In this work the sequence of computations is called EUBL. It is as follows:

1) EUL1: Solution of Euler equations with

$$[v^3_{\text{inv}}]_{\text{wall}} = 0 \tag{4}$$

2) BL1: First-order boundary-layer calculation

3) EUL2: Solution of Euler equations with

$$[\rho_{\text{inv}} v^3_{\text{inv}}]_{\text{wall}} \neq 0 \tag{5}$$

4) BL2: Second-order boundary-layer calculation.

EUBL—Euler Solver

For the computation of the inviscid solutions EUL1 and EUL2, the program CEVCATS is used.[11] CEVCATS solves the unsteady, three-dimensional Euler equations written in integral form using the finite-volume approach. Central discretization for convective flux approximation, in conjunction with a dissipative operator including a blend of second and fourth differences, is used. On smooth meshes the discretization error is of second-order accuracy. Near shocks, the accuracy is switched locally to first-order due to numerical dissipation. The classical Euler wall boundary condition has been changed such that, if necessary, wall-normal velocity components are allowed.

Integration in time of the resulting system of ordinary differential equations is performed by means of an explicit Runge-Kutta scheme.

For the purpose of CPU efficiency, local time stepping and implicit residual damping are used. In supersonic flow regimes a space-marching version of CEVCATS is used. CEVCATS is written in block structured form.

Although the test flow is axisymmetric, the three-dimensional version of CEVCATS is used. This makes it possible to get a feeling for CPU-time requirements that can be expected for more general flow cases in the future.

EUBL—Boundary-Layer Solver

For computing the boundary-layer solutions BL1 and BL2, the program SOBOL is used.[9,10] SOBOL solves the three-dimensional, compressible, second-order boundary-layer equations formulated in surface oriented locally monoclinic coordinates. x^1, x^2 are locally parallel to the surface, x^3 is rectilinear and normal to it.

In the first-order boundary-layer mode, curvature effects are neglected and the classical outer-edge boundary condition is used.

In the second-order boundary-layer mode, curvature terms are explicitly included in the equations. Furthermore, second-order patching conditions (3) are used as outer-edge boundary-layer conditions.

SOBOL solves the second-order boundary-layer equations using a finite difference method. Either the zig-zag, the rectangular, or the double zig-zag scheme is used, depending on criteria for stability and efficiency. Discretization of the equations is of second-order accuracy. Space-marching in both wall-parallel directions reveals the method as implicit only in wall-normal direction. Therefore, a nonlinear algebraic system of equations is solved for each of the wall normals. This procedure has the advantage that numerical problems at one wall-normal do not necessarily lead to a breakdown of the whole solution process. It can be continued neglecting only that special wall-normal. Computation of δ is part of the iterative solution process of the system of equations.

Viscosity is computed by means of the dimensionless Sutherland law or by means of a composite law. For the latter it depends on T_{ref} and the local temperature within the boundary

layer, which combination of a dimensional linear law and the dimensional Sutherland law is employed to calculate dimensionless viscosity. For low temperatures the following dimensional, linear law is used[12]:

$$\mu = 0.693873 \times 10^{-7} \cdot T \qquad T < 110.4 \text{ K} \qquad (6)$$

As initial solution a generalized stagnation point solution applied at each station of the starting interval is used.

Stability and Transition Prediction

For computing the stability behavior the program COSMET is used.[12] COSMET solves the linear stability equations of compressible, parallel, three-dimensional flow along curved surfaces. These equations are derived from the tensor-analytical form of the Navier-Stokes equations formulated in orthogonal, curvilinear coordinates. The flow is split into a steady mean flow and an unsteady disturbance. In addition, the so-called parallel-flow assumption is made. It states that mean flow derivatives are only taken into account in wall-normal direction. Therefore, the history of the flow is neglected. In addition, the wall-normal velocity component within the boundary layer is assumed to be zero. Perturbations are assumed as single, normal modes.

The assumptions are substituted into the Navier-Stokes equations, and nonlinear terms are neglected. Finally, an order-of-magnitude analysis is made where only terms of larger order than $\mathcal{O}(Re^{-1/2})$ are retained. The procedure leads to a system of five coupled, ordinary differential equations of eighth order.

The approach in COSMET is a so-called local boundary-value method. The equations are discretized by means of a Chebyshev-collocation method and solved employing LU-decomposition and Gauss elimination. COSMET is capable of calculating temporal as well as spatial eigenvalues. Furthermore, several strategies to compute N factors are implemented.[3,12]

Second-mode waves are most unstable as two-dimensional waves. In other words, for second-mode waves, Ψ plays no role. In the special case of an axisymmetric mean flow the waves are most amplified if the crests propagate in x^1 direction. Therefore, N-factor calculation reduces to

$$N = \max_f \left[\left(\ln \frac{A_1}{A_0} \right)_f \right] = \max_f \left[-\int_{(x^1)_0}^{(x^1)_1} \alpha_i \, \mathrm{d}x^1 \right] \qquad (7)$$

In COSMET the same viscosity laws are used as in SOBOL.

Geometry, Grid and Conditions

Table 1 summarizes important geometry data. Figure 1 shows parts of the grid used for Euler calculations. The grid size is 161/41/31 points in $i/j/k$ direction. Twenty-one grid points were used to discretize the nose in i direction. In the i and j direction a linear stretching of the grid spacing was introduced. The reason for doing this in the i direction is efficiency, whereas the reason in the j direction is as follows. Inviscid super- and hypersonic flows around blunt configurations are mainly characterized by the detached shock wave in front of the body. Within the shock layer the entropy is constant along streamlines (e.g., the body), but varies from one streamline to another due to shock curvature. This leads to the so-called entropy layer that may be swallowed by the boundary layer far downstream. To resolve this thin entropy layer one has to provide for a sufficient number of grid points near the wall. For computing the far field, Billig's correlation was used.[13]

Table 1 Geometry

Nose shape	RN	RN/L	Θ_c
Spherical	0.00381	0.00375	7

Table 2 Calculation of Re_∞ using different viscosity laws

Dimensional viscosity law	T_∞	$\mu_\infty \times 10^6$	ρ_∞	Re_∞
Sutherland	54.348	3.55153	0.02653	33,641
Linear	54.348	3.77106	0.02653	31,683

Table 3 Condition for EUBL mean-flow calculation

Dimensionless viscosity law	M_∞	T_∞	ρ_∞	Re_∞	Pr
Sutherland	8	54.348	0.02463	31,250	0.72

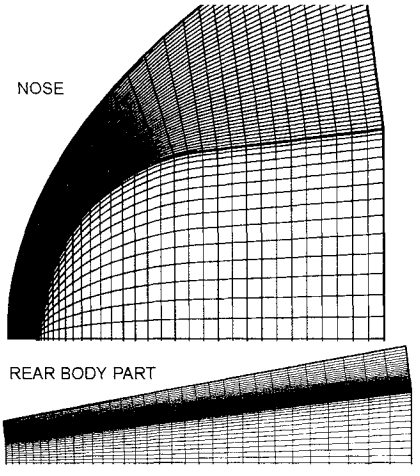

Fig. 1 Test configuration, Euler grid.

All boundary-layer calculations have been conducted with 121 points in wall-normal direction using the Euler surface grid.

SOBOL needs dimensional reference conditions as input for computing the Reynolds number Re_{ref}. Calculating Re_{ref} using experimental test conditions and Sutherland's law leads to a 7% larger Reynolds number than the experimental value of 31,250.[4] The reason is that Sutherland's law is not suitable for extremely low temperatures like $T_\infty = 54.348$ K. Using the linear viscosity law (6) the difference is only about 1% (see Table 2).

However, both Esfahanian and Kufner used the dimensionless Sutherland law. To be able to compare with their results this law is valid for all results presented here, with the exception of case 3 of the sensitivity study. To keep $Re_\infty = 31{,}250$, ρ_{ref} was adjusted. Table 3 summarizes the conditions. The values of M_∞, T_∞, Re_∞, and Pr are used in Refs. 5 and 7 as well.

Results and Discussion

EUBL Mean-Flow Results

Figures 2a and 2b show second-order temperature profiles and their second derivatives at $b/RN = 17.8$. Both are in very good agreement with Kufner's solution. At $b/RN = 175$, small differences exist between Kufner's and Esfahanian's solution, as well as compared to the EUBL result. All three calculations predict the same maximum of second derivative, but at slightly different locations in wall-normal direction (Figs. 3a and 3b). $Re_{x,e}$ predicted by EUBL deviates from $Re_{x,e}$, predicted by the experiment of Stetson et al.[4] roughly 3%.

About 1 h CPU-time on a Cray Y-MP was necessary to compute the EUBL calculation presented here. CEVCATS is able to run in the TLNS mode also. EUBL would be at least seven times as fast as the three-dimensional TLNS code. This estimate relies on known CPU-time requirements per time step and grid point for the TLNS mode and on a Navier-Stokes grid containing 161/101/31 points in $i/j/k$-directions. Furthermore, the Euler convergence rate is assumed.

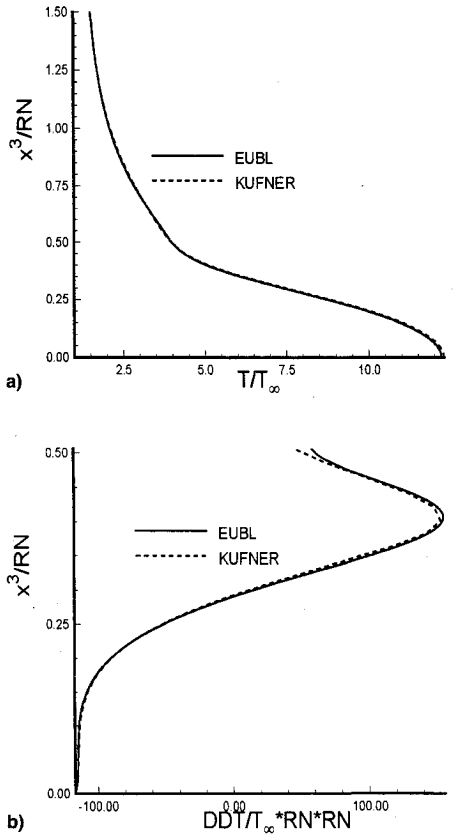

Fig. 2 a) Temperature profile, comparison with references, b/RN = 17.88 and b) second derivative of temperature profile, comparison with references, b/RN = 17.88.

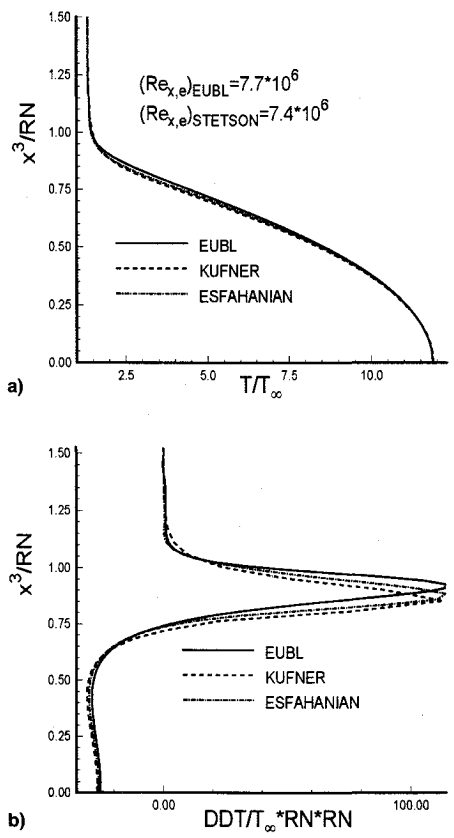

Fig. 3 a) Temperature profile, comparison with references, b/RN = 175.03 and b) second derivative of temperature profile, comparison with references, b/RN = 175.03.

EUBL-Based Stability Results

Figure 4 shows spatial amplification rates of two-dimensional, second-mode waves at b/RN = 175 as a function of frequency. The amplification on the basis of EUBL mean-flow calculations is in qualitative agreement with those of Esfahanian,[5] Malik et al.,[6] and Kufner.[7] EUBL-based stability results predict the same large differences between theory and experiment already shown in the references, which may be due to nonlinear effects.[14] Although all theoretical results are qualitatively similar, differences remain. The maximum amplification rate is somewhat lower than Esfahanian's, and approximately 7% higher compared to the result of Malik et al. The frequency of the maximum amplification rate is in good agreement with the result of Esfahanian, and differs from the result of Malik et al. by less than 5%.

The differences between the EUBL-based and Kufner's results are caused by mean-flow differences, because in both cases COSMET was used. The difference compared to the result of Esfahanian might be caused by both different mean flows and different stability codes. Therefore, spatial amplification rates for Esfahanian's mean flow at b/RN = 175 were calculated with COSMET. Figure 5 shows that COSMET calculated the same result as Esfahanian's stability code. Again, differences in stability behavior are caused by different mean flows. In the case of the result of Malik et al. it could not be clarified whether different mean flows or different stability codes are responsible for the differences, because there remained some uncertainties concerning Prandtl number and viscosity law used in Ref. 6.

Figure 6 shows curves of spatial amplification rate over $Re_{x,\infty}$. Along each curve f is held constant. Curves for frequencies from 100 to 150 kHz and Malik's curve of maximum amplification are shown. Differences compared to EUBL-based stability results are about 10%. Figure 7 shows results

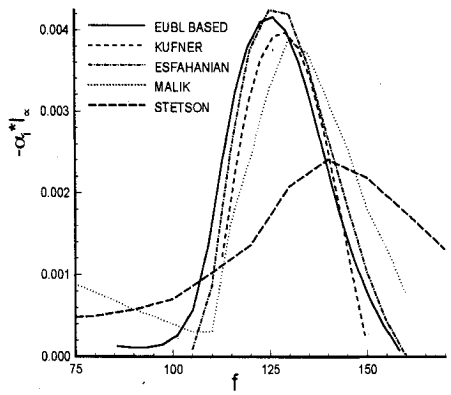

Fig. 4 Spatial amplification rates, second mode, Ψ = 0, comparison with references, b/RN = 175.03.

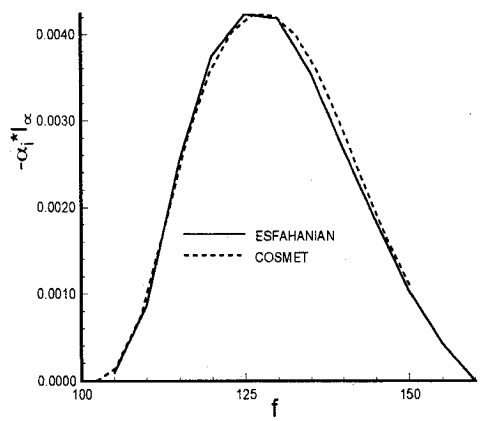

Fig. 5 Spatial amplification rates, second mode, Ψ = 0, influence of different stability codes.

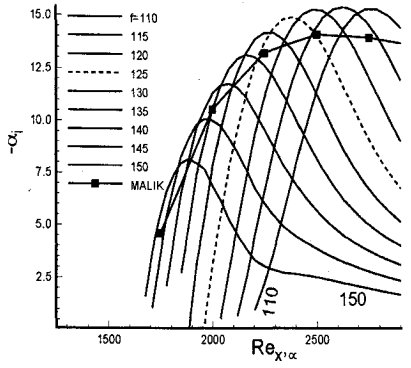

Fig. 6 f = const curves of spatial amplification, second mode, Ψ = 0, comparison with references.

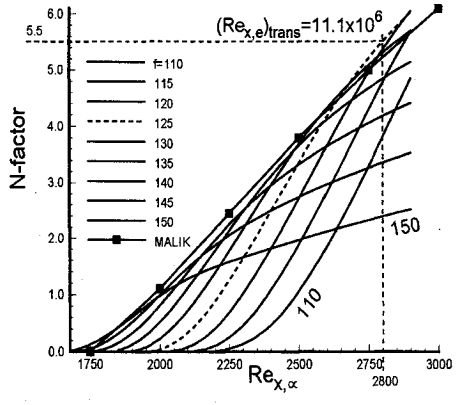

Fig. 7 Transition location, second mode, Ψ = 0, comparison with references.

of N factor calculations. Up to N factors of 6 the envelope is in good agreement with the result of Malik et al.

Malik et al. also investigated the stability behavior of a sharp-cone boundary layer at $M_\infty = 8$ and $\alpha = 0$ deg. Comparing these results with the experimental data of Stetson et al.,[4] $N = 5.5$ was found. Since the blunt cone experiments were conducted in the same wind tunnel, $N = 5.5$ was also assumed in this case. Transition took place at $Re_{x,\infty} = 2800$ ($Re_{x,e} = 11 \times 10^6$).[6] Using the same N factor, EUBL-based results lead to the same transition location. The frequency range of interest around $N = 5.5$ corresponds to Malik's result and is between 120–130 kHz.

In contrast to the differences concerning spatial amplification, the computed transition location differs from the estimate of Stetson ($Re_{x,e} \approx 13 \times 10^6$) by only about 15%. In this context it should be emphasized that Stetson's estimate relies on experiences from experiments in which bluntness effects on transition location were studied (not the effects on stability behavior).

Sensitivity

Case 1: Effect of Viscous-Inviscid Interaction

To compute a second-order boundary layer neglecting viscous-inviscid interaction, EUBL reduces to a two-step method, consisting of EUL1 and BL2. Figure 8 shows the result compared to the complete EUBL result at $b/RN = 175$. The profile without displacement effect is more unstable for frequencies higher than 120 kHz (see Fig. 9). The higher the frequencies are, the larger the percentage difference is. This tendency is confirmed when looking at differences between constant frequency curves of spatial amplification (see Fig. 10). In the lower frequency range between 110–125 kHz, differences of about 10% exist only far downstream. Comparing curves of higher frequencies leads to differences of the order 100% over the whole range of $Re_{x,\infty}$ (e.g., $f = 150$). However, Fig. 11 shows that the difference in transition lo-

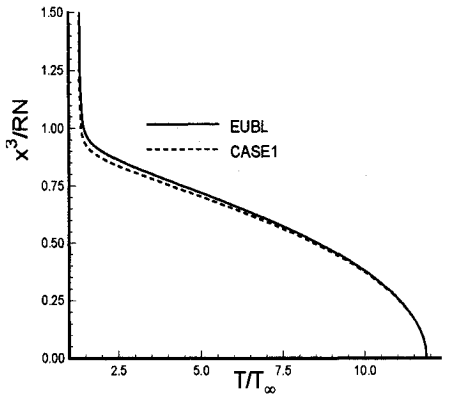

Fig. 8 Temperature profile, case 1: Effect of viscous-inviscid interaction, b/RN = 175.03.

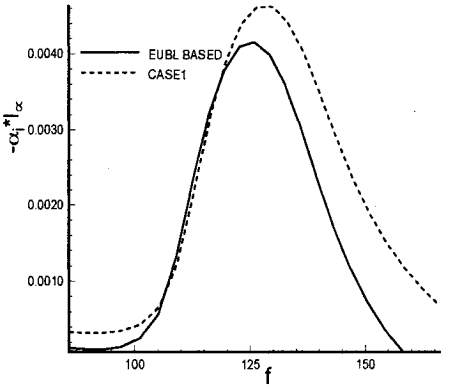

Fig. 9 Spatial amplification rates, second mode, Ψ = 0, case 1: effect of viscous-inviscid interaction, b/RN = 175.

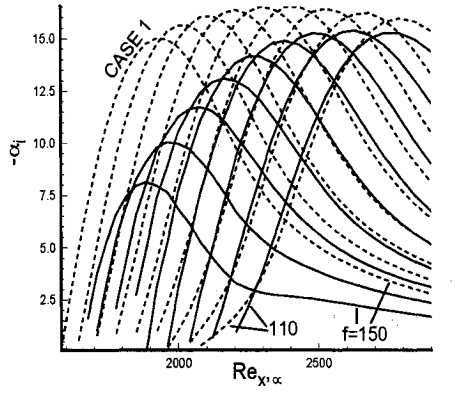

Fig. 10 f = const curves of spatial amplification, second mode, Ψ = 0, case 1: effect of viscous-inviscid interaction.

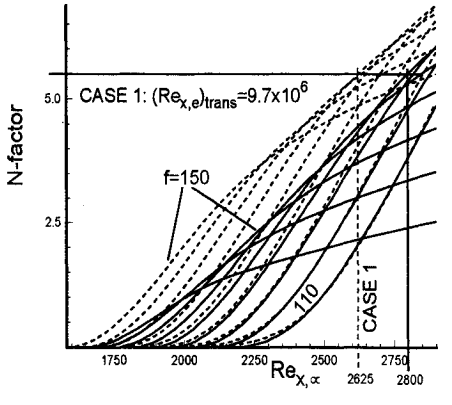

Fig. 11 Transition location, second mode, Ψ = 0, case 1: effect of viscous-inviscid interaction.

Table 4 Condition for EUBL mean-flow calculation, case 3

Dimensionless viscosity law	M_∞	T_∞	ρ_∞	Re_∞	Pr
Composite	8	54.348	0.02616	31,250	0.72

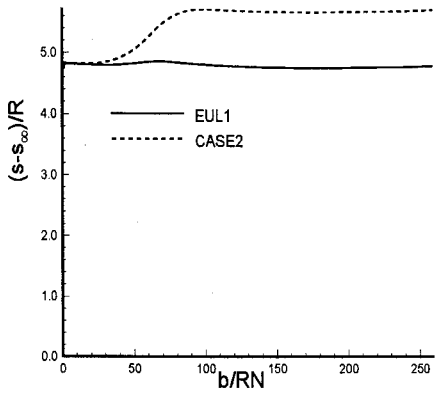

Fig. 12 EUL1 entropy at wall, case 2: effect of entropy-layer resolution.

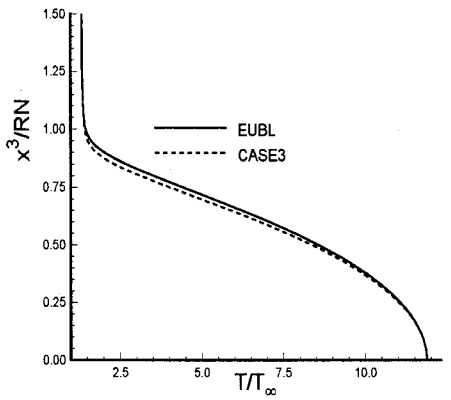

Fig. 13 Temperature profile, case 3: effect of composite viscosity law, b/RN = 175.03.

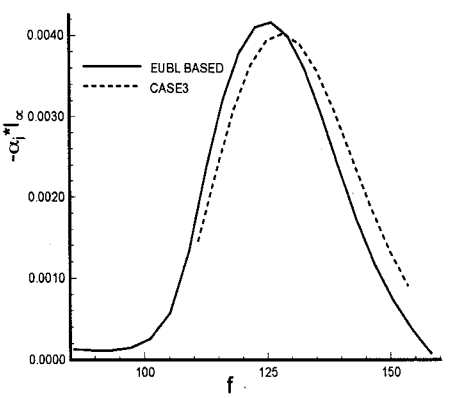

Fig. 14 Spatial amplification, second mode, Ψ = 0, case 3: effect of composite viscosity law, b/RN = 175.03.

cation $Re_{x,c}$ for N = 5.5 is merely about 10% ($Re_{x,\infty} \approx 2625$, $Re_{x,c} \approx 9.7 \times 10^6$), because for N = 5.5, the highest second-mode frequencies play no role. But keep in mind that the difference in transition location also depends on the N factor used and on the gradients of the computed envelopes. Therefore, investigating other flow cases may change the situation.

Case 2: Effect of Entropy-Layer Resolution

Provided that the Euler solution EUL1 is grid-converged, resolution of a thin entropy layer as well as inviscid wall values still depend on the amount of numerical dissipation.

Figure 12 shows that increasing the amount of numerical dissipation in EUL1 increases the entropy at the wall considerably. The same effect is present when comparing internal energy and density. However, these properties are used as input for the first-order boundary-layer computation BL1, which provides the source distribution for EUL2. Consequently, each step of EUBL is influenced. In this case, the effect of increased numerical dissipation in EUL1 on the EUBL mean flow, stability, and transition location is about the same as the effect of neglecting viscous-inviscid interaction. Again, transition location is shifted upstream about 10%.

Case 3: Effect of Composite Viscosity Law

From a physical point of view it seems to be more realistic to use the composite viscosity law, because the reference temperature is small. In contrast to previous results concerning EUBL, stability, and transition location, this law is used now. Table 4 summarizes the conditions.

The composite law changes the temperature profile at b/RN = 175 as shown in Fig. 13. The consequence of this is that spatial amplification rates are shifted to somewhat higher frequencies, and that the difference between maximum values of spatial amplification is less than 5% (see Fig. 14). As far as transition location is concerned, negligible differences were found.

Conclusions

Transition location for a hypersonic, axisymmetric boundary layer was calculated from an engineering point of view using an Euler/boundary-layer method, including second-order boundary-layer theory called EUBL and local, linear stability theory together with the e^N method. As test configuration, a blunt, slender cone at M_∞ = 8 and α = 0 deg was chosen. Both mean flow and stability results have been compared with available theoretical as well as experimental data. Furthermore, the sensitivity of the procedure was investigated.

Computation of stability behavior and transition location on the basis of EUBL leads to results comparable to those based on Navier-Stokes mean flows. Differences in theoretical stability results presented here are mainly caused by different mean flows, not by different stability codes. As far as efficiency is concerned, EUBL is capable of computing steady, laminar mean flows at significantly less cost than a corresponding Navier-Stokes code. The efficiency of EUBL may be important for industrial applications.

Using EUBL, or a similar boundary-layer method, there may be problems if entropy-layers over blunt, slender configurations are not resolved properly in EUL1, because EUL1 wall values influence each step of the complete EUBL procedure. Proper resolution requires a sufficiently fine grid and as low numerical dissipation as possible. Furthermore, the effect of viscous-inviscid interaction needs to be considered. If it is assumed to play no role, CPU-time requirements decrease further. In the work presented here, neglecting viscous-inviscid interaction and improper resolution of the entropy layer shifted transition location about 10% upstream.

Employing a composite viscosity law instead of the dimensionless Sutherland law had less effect than expected.

Acknowledgments

The author wants to thank Norbert Kroll, Francois Monnoyer, Uwe Dallmann, and Ewald Kufner for providing the codes and helpful discussions. Thorwald Herbert kindly provided the mean-flow solutions of Vahid Esfahanian.

References

[1]Van Dyke, M., *Perturbation Methods in Fluid Mechanics*, Annotated ed., Parabolic Press, Stanford, CA, 1975, pp. 77–97.

[2]Aupoix, B., Brazier, J. Ph., Cousteix, J., and Monnoyer, F., "2nd-Order Effects in Hypersonic Boundary Layers," 3rd Joint Eu-

rope/U.S. Short Course in Hypersonics, Univ. of Technology, Aachen, Germany, Oct. 1990.

[3]Arnal, D., "Boundary-Layer Transition: Prediction Based on Linear Theory," Special Course on Progress in Transition Modelling, AGARD Rept. 793, Brussels, Belgium, March 1993.

[4]Stetson, K. F., Thompson, E. R., Donaldson, J. C., and Siler, L. G., "Laminar Boundary-Layer Experiments on a Cone at Mach 8, Part 2: Blunt Cone," AIAA Paper 84-0006, Jan. 1984.

[5]Esfahanian, V., "Computation and Stability Analysis of Laminar Flow over a Blunt Cone in Hypersonic Flow," Ph.D. Dissertation, Ohio State Univ., Columbus, OH, 1991.

[6]Malik, M. R., Spall, R. E., and Chang, C.-L., "Effect of Nose Bluntness on Boundary-Layer Stability and Transition," AIAA Paper 90-0112, Jan. 1990.

[7]Kufner, E., Dallmann, U., and Stilla, J., "Instability of Hypersonic Flow past Blunt Cones-Effects of Mean Flow Variations," AIAA Paper 93-2983, July 1993.

[8]Wüthrich, S., "Numerical Simulation of Non-Equilibrium Chemically Reacting Hypersonic Flows by Means of a Coupled Euler/Boundary-Layer Method," Thesis 1096, Technical Univ. of Lausanne, Inst. of Mechanics, Lausanne, Switzerland, 1992.

[9]Monnoyer, F., "SOBOL Mk 2.3 Handbook," Deutsche Aerospace AG (DASA), DASA-LME211-Aero-MT-NM-931, Munich Germany, Oct. 1992.

[10]Monnoyer, F., "Calculation of Three-Dimensional Attached Viscous Flow on General Configurations Using 2nd-Order Boundary-Layer Theory," *Journal of Flight Science and Space Research*, Vol. 14, 1990, pp. 95–108.

[11]Streit, Th., Kroll, N., and Schöne, J., "Finite-Volume Discretization for the Solution of Three-Dimensional Euler Equations for High Speed Flows," German Aerospace Research Establishment (DLR), Inst. of Design Aerodynamics, IB 129-91/06, Braunschweig, Germany, Oct. 1991.

[12]Simen, M., "COSMET, a DLR-DORNIER Computer Program for COmpressible Stability Analysis with Local METric," DLR, Inst. of Theoretical Fluid Mechanics, IB 221-91 A 09, Göttingen, Germany, Jan. 1991.

[13]Anderson, J. D., "Hypersonic and High Temperature Gas Dynamics," *McGraw-Hill Series in Aeronautical and Aerospace*, McGraw-Hill, New York, 1989, pp. 189–192.

[14]Chang, C.-L., and Malik, M. R., "Non-Parallel Stability of Compressible Boundary Layers," AIAA Paper 93-2912, July 1993.